Bioresource Technology Reports 34 (2026) 102746

Contents lists available at ScienceDirect

Bioresource Technology Reports

journal homepage: www.sciencedirect.com/journal/bioresource-technology-reports

Bioelectrochemically assisted constructed wetlands for municipal wastewater treatment and the suitability of different biochar materials as system media

Laura Tarvainen [a,*], Katharina Kujala [a,b], Hellen Silva Santos [c], Maarit Liimatainen [b], Elisangela Heiderscheidt [a]

[a] Water, Energy and Environmental Engineering Research Unit, Faculty of Technology, 90014, University of Oulu, Finland
[b] Natural Resources Institute Finland, Paavo Havaksen tie 3, Oulu, FI-90570, Finland
[c] Fibre and Particle Engineering Research Unit, Faculty of Technology, 90014, University of Oulu, Finland

ARTICLE INFO

Keywords:
Metland technology
Nature-based solutions
Sanitation
Wastewater treatment

ABSTRACT

Microbial electrochemical technology constructed wetlands (METlands) use electroconductive (EC) materials in place of inert substrates such as gravel to enhance pollutant removal. This study evaluated whether EC biochar produced from waste biomass (olive pit, wood pellet, and woodchip) could function as an alternative METland media, an area with limited prior research. Biochars were tested in up-flow columns and compared with coke, a commonly used high-EC medium, and gravel, the typical inert substrate in conventional wetlands. Pollutant removal performance, material properties, biofilm-associated bacterial communities, and gas fluxes were assessed. Biochar and coke generally achieve higher removal of chemical oxygen demand (COD), nitrogen, phosphorus, and selected micropollutants than gravel, indicating that EC biochar can serve as a suitable METland medium. Electroactive bacteria were present at low relative abundance but were highest in biochar systems. Biochar columns also showed higher CO_2, N_2O, and CH_4 fluxes, though these patterns are only indicative due to limited GHG measurements, and further research is needed to clarify greenhouse gas emissions.

1. Introduction

Nature-based solutions (NBSs) address various societal challenges using ecosystems and natural processes, solving important issues such as wastewater management (Cross et al., 2021). Among the NBSs used in wastewater treatment, constructed wetlands (CWs) are the most commonly utilised. Their capacity to treat wastewater from different sources has been well-demonstrated, both in research and real applications (Dotro et al., 2017; Cross et al., 2021; Vymazal, 2023). Thus, CWs are considered to be sustainable NBS alternatives to grey wastewater treatment infrastructure. However, CW implementation can also have drawbacks, including operational issues like their relatively high area demand, media clogging, and reduced performance under cold climate conditions (Kadlec and Wallace, 2008; Cross et al., 2021). Furthermore, stricter regulations, such as the revised European Commission Urban Wastewater Treatment Directive (Directive (EU) 2024/3019, 2024), have increased pressure on operators and the systems used to meet requirements, including a requirement to remove emerging contaminants (e.g., pharmaceutical compounds). Therefore, the need persists for NBS technology development and validation to meet environmental protection goals as well as sustainability and societal benefit targets.

A novel approach to CW technology was introduced by Yadav et al. (2012). It was based on microbial fuel cell (MFC) principles. MFCs are bioelectrochemical systems in which microorganisms like electroactive bacteria (EAB) oxidize organic and inorganic matter and transfer electrons to electroconductive materials, converting chemical energy into electricity (Logan and Regan, 2006). Because CW–MFC systems offer the potential for simultaneous wastewater treatment and energy generation, most studies following Yadav et al. (2012) have focused on their technical performance and energy recovery potential (Doherty et al., 2015). However, MFCCWs still cannot produce energy cost-effectively (Roy et al., 2023). Aguirre-Sierra et al. (2016) therefore proposed shifting the focus from energy recovery to pollutant removal by replacing traditional media with electroconductive materials and removing external circuits, resulting in the “microbial electrochemicalbased constructed wetland (METland®).” In METland (MET) systems, EAB oxidize reduced

* Corresponding author.
E-mail address: laura.tarvainen@oulu.fi (L. Tarvainen).

https://doi.org/10.1016/j.biteb.2026.102746
Received 17 December 2025; Received in revised form 30 March 2026; Accepted 6 April 2026
Available online 7 April 2026

compounds and transfer electrons to solid electroconductive materials that act as unlimited electron acceptors (Aguirre-Sierra et al., 2016).

Based on studies reported to date, METs represent a powerful hybrid technology that can outperform conventional CWs (Du et al., 2022; Peñacoba-Antona et al., 2022). Published reports suggest that these systems can enhance biodegradation rates of organics, allowing the reduction of the area requirements of conventional CWs (Ramírez-Vargas et al., 2018; Prado de Nicolás et al., 2022; Wei et al., 2025). Decreased clogging and generally higher (although variable) nitrogen (N) removal compared to CWs have also been reported (Aguirre-Sierra et al., 2016; Ramírez-Vargas et al., 2018; Prado et al., 2020; Wei et al., 2025). Should the high efficiencies and low energy requirements of METs be confirmed, they could serve as ideal alternative treatment solutions within the realm of NBS (Peñacoba-Antona et al., 2021; Vymazal et al., 2021).

Most studies investigating METs have used carbon-based electric conductive (EC) materials as the system media due to their high specific surface area (As) and EC properties (Ramírez-Vargas et al., 2018). While investigating the performance of different EC materials (graphite, coke, and wood biochar), Prado et al. (2019 and 2020) reported that the wood-derived biochar tested was the most efficient. This was despite the EC (ca 0.4 mS/cm) being between 40 and 40,000 times lower than the coke and graphite materials used, respectively. The authors concluded that EC was not the only material property promoting the development of EAB-based biofilms in METs, a conclusion that is supported by recent studies (Prado de Nicolás et al., 2022). The higher biodegradation performance of the biochar tested has been attributed to the electroactive oxygen functionalities on the material surface (Prado et al., 2019, 2020; Prado de Nicolás et al., 2022). However, the properties of biochar that support EAB activity and the suitability of biochar produced from different biomass sources as media in MET systems have not been investigated to date. Furthermore, only a limited number of studies have reported on MET systems in general. Thus, research is still needed to clarify contaminant retention pathways, linked gas emissions and the influence of the material used on biofilm formation and overall system functioning and efficiency (Vymazal et al., 2021; Prado de Nicolás et al., 2022). More specifically, persisting knowledge gaps recognised considering MET systems are, e.g., (i) the role of surface chemistry versus the electrical conductivity of materials on microbial community development, (ii) effects of biomass feedstock on biochar properties and system performance, (iii) GHG emissions under different operating conditions and trade-offs with organics and nitrogen removal efficiency and (iv) micropollutant removal capabilities and the contribution of physical, chemical and biological processes on overall contaminant removal.

Aiming to fill some of the identified knowledge gaps, the main goal of this study was to expand the research on EC biochar materials as suitable media for MET systems and to produce further evidence of MET systems' capabilities. The novelty of this work lies in testing EC-biochar materials produced from different waste biomasses, possessing different properties to the only wood-based material tested to date, while comparing them with coke (a high-EC reference material) and gravel (a conventional CW medium). Moreover, the study evaluated pollutant removal efficiency and assessed performance differences using a wide range of water quality and operational parameters. The bacterial communities developed on each material were also characterized. The removal of micropollutants and greenhouse gas (GHG) emissions was explored during selected monitoring events, providing additional insights into the performance of the different materials, the processes occurring within the systems, and potential factors influencing system functionality. By combining pilot-scale operation, multi-material comparison, micropollutant analysis, microbial community profiling, and gas flux measurements, this study provides further evidence for the use of EC-biochar as media in MET type of systems.

2. Materials and methods

The experimental setup consisted of testing inert filler material (i.e. gravel) alongside four different EC materials (coke and three biochars generated from waste biomasses: olive pits, wood pellets, and woodchips) in flow-through columns operating as pilot wetland systems. The pilots ran for a total operation time of 32 weeks, of which the first 6 weeks were identified as the system's stabilization phase based on preliminary nutrient removal measurements and redox readings, which stabilized around week 6 (stable COD removal efficiency $\geq$60% and stable redox gradient, Supplementary material Fig. S1 and Fig. S2).

2.1. Pilot systems dimensions and set-up

Up-flow columns were constructed from polyvinylchloride (PVC) cylinders (diameter 10 cm, height 60 cm, surface area 78.5 cm^2, total volume 4.7 L) and operated indoors at the University of Oulu laboratory facilities (Finland), where temperature was maintained at 19.8 $\pm$ 1.2 °C. The columns operated as plant-free microbial electrochemical-based CW units, with the conductive bed serving as the anode and the oxygen-exposed upper layer as the cathode, operating without an external circuit. To ensure experimental consistency, three replicates were prepared for each of the three biochar materials, while coke and gravel were tested in duplicate, resulting in a total of 13 columns. A perforated PVC pipe (diameter 1.5 cm) was positioned centrally in each column to allow sensor placement. Porewater sampling ports were installed 22.5 cm above the column base, fitted with Rhizon collectors (pore size 0.15 µm). To prevent flotation of the media, a thin perforated PVC plate was placed above the material surface. A detailed schematic of the column design is presented in Fig. 1.

Primary treated wastewater (WW) was collected from the outflow of the primary clarifier at the Taskila wastewater treatment plant (WWTP, 180,000 PE, Oulu, Finland). WW was introduced to the bottom of the columns using multichannel peristaltic pumps (Gilson Minipuls 3; Watson Marlow 205S). Biweekly, new 30 L batches were collected and stored at 5–8 °C. Before testing, the wastewater was transferred to a 60 L bucket at room temperature, from which it was supplied to the systems. To minimize sedimentation, a bilge pump mixed the contents for 15 min each hour. A mesh filter was installed on the inflow lines to prevent clogging by large particles. The flow rate was maintained at 0.5 mL/min (0.72 $\pm$ 0.06 L/d), monitored weekly by measuring the outflow, and adjusted as needed. The water level was kept constant at 50 cm, fully submerging the media. Hydraulic retention times (HRT) varied with material porosity: olive pit 71.7 h (2.99 d), wood pellet 81.9 h (3.42 d), woodchip 80.8 h (3.36 d), coke 71.7 h (2.99 d), and gravel 65.3 h (2.72 d). One replicate per material contained two oxidation/reduction potential (ORP) sensors (Ecotech GmbH, platinum redox electrode with Ag/AgCl reference, art. no. 461) at 22.5 cm and at the bottom; other replicates had one bottom sensor. All columns included a reference sensor ~2 cm below the water surface.

2.2. Wastewater characteristics and sampling

To assess system efficiency, inflow and outflow samples were collected weekly or biweekly throughout the experiment. HRT was accounted for by taking inflow samples 2–3 days before outflow sampling. Outflow samples were obtained by clipping the outflow pipes 16–18 h beforehand to raise water levels and ensure sufficient treated volume, after which samples were collected from the surface using a glass pipette. Inflow samples were taken with a pump placed in the storage bucket, using an intake pipe fitted with the same protective mesh as the column inflow.

Inflow and outflow samples were analysed in-house using a HACH DR1900 Portable Spectrophotometer (HACH Company, Loveland, CO, USA) for total nitrogen (Tot-N, LCK338, 20–100 mg/L), total phosphorus (Tot-P, LCK348, 0.5–5 mg/L), and chemical oxygen demand

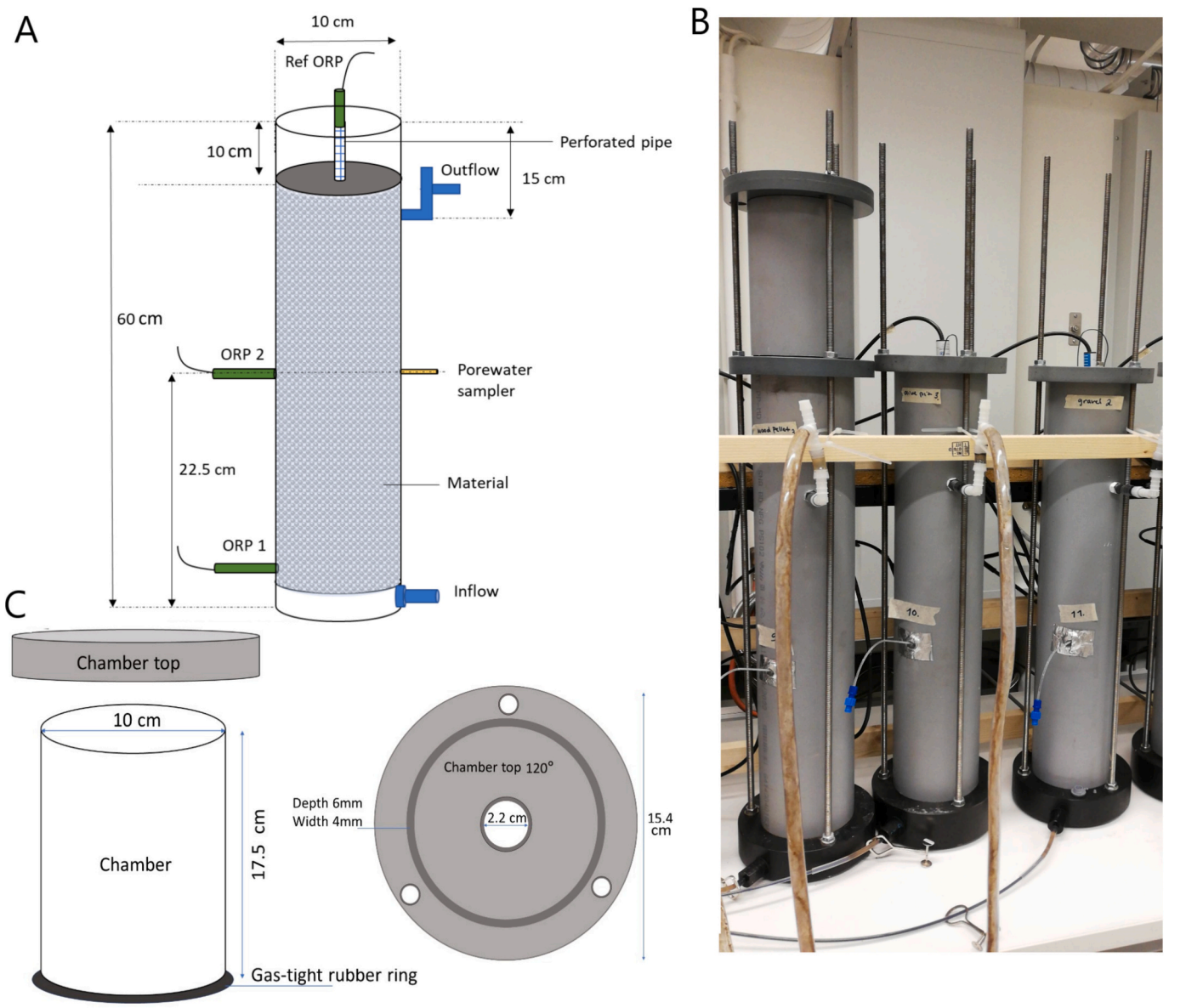

Fig. 1. Schematic drawing of the pilot system (A); a picture of the actual experimental setup with the gas chamber on one of the columns (B); and a schematic drawing of the gas chamber design (C).

(COD, LCK514, 100–2000 mg/L; LCK314, 15–150 mg/L), and with a YSI 9500 Photometer (YSI Inc., Yellow Springs, OH, USA) for ammonium nitrogen (NH_4^+-N, 0–1 mg/L), phosphate phosphorus (PO_4^{3-}-P, 0–4 mg/L), alkalinity, and nitrate nitrogen (NO_3^--N, 0–20 mg/L), using kits selected according to concentration ranges and product availability.

The use of reagent kits from different suppliers for the analysis of fractions of the same compound is recognised as a methodological limitation. In the case of phosphorous analysis, e.g., tot-P concentrations measured were on some occasions lower than those measured for PO_4-P in the same samples (Table 1). Pointing to a possible divergence between the reagents (kits) used. Cross-checking of the data did not identify inconsistencies in the measurements of other parameters. Chemical oxygen demand was analysed at every event, while nitrogen and phosphorus fractions were measured in ~65% of events due to cost and equipment constraints, following instrument and reagent kit manuals. During GHG sampling weeks (Section 2.3), samples were also sent externally for total organic carbon (TOC) analysis. Electroconductivity (EC), dissolved oxygen (DO), pH, and temperature were monitored using a handheld multiparameter sonde (Xylem WTW, 350i), turbidity with a Lovibond TB 211IR meter. To assess micropollutant removal, one set of samples (week 31) was analysed at the Povodí Vltavy State

Table 1
Inflow wastewater characteristics. Data represents the average values followed by (±) standard deviation within the "n" number of samples.

Wastewater			
Parameter	Inlet	Unit	n
COD	341.3 ± 253.0	mg/L	14
Alk	530.0 ± 251.8	mg/L	10
Tot P	4.1 ± 3.7	mg/L	13
PO_4-P	4.2 ± 2.3	mg/L	11
Tot N	61.2 ± 23.9	mg/L	14
NH_4^+-N	61.6 ± 22.5	mg/L	11
NO_3^--N	5.3 ± 2.9	mg/L	10
Turbidity	37.2 ± 23.2	NTU	24
EC	109.7 ± 13.8	mS/cm	24
DO	1.3 ± 1.1	mg/L	24
pH	7.6 ± 0.2		24

Enterprise laboratory (Czech Republic) for 120 pharmaceuticals and personal care products using liquid chromatography tandem mass spectrometry (LC-MS/MS).

The wastewater quality fed to the pilot systems varied considerably throughout the experimental period, largely due to normal fluctuations in real WWTP influent and additional changes occurring during the 1–2-week storage period. The average values of the monitored parameters in terms of inflow wastewater characteristics, as well as the determined standard deviation and number of samples (n), are provided in Table 1.

2.3. Greenhouse gas collection and analysis

Emissions of CO_2, CH_4, and N_2O were measured using the non-steadystate static chamber method (Fiedler et al., 2022). GHG measurements were conducted during two campaigns (weeks 22 and 25), coinciding with inflow and outflow sampling. The chamber consisted of a PVC body (17.5 cm) and lid, fitted to the column tops with butterfly screws and gastight rubber hoops (Fig. 1). After sealing the chambers, the first gas sample was taken immediately, followed by samples every 10 min over 30 min (four samples per chamber). Gas was withdrawn with hypodermic needles and syringes. The sampling pipe was flushed before collecting a 20 mL sample, which was injected into preevacuated vials. Concentrations of CO_2, CH_4, and N_2O were analysed by gas chromatography (HP 8890 Series GC System, Agilent, USA) at the Natural Resources Institute Finland (LUKE) laboratory in Oulu.

2.4. Materials tested and their characterization

Pre-washed gravel was obtained from a local construction supplier, and the charcoalbased coke material from Suomen Kotteria Oy. Biochar products were provided by Carboculture (production details available on their website). All materials were sieved to a 4–20 mm particle size using metal sieving pans. Bulk porosity (φ) was measured volumetrically by adding water to a known volume of packed media (V_{sample}) and recording the volume of water (V_{water}) required to fill the void space (three replicates per media type). HRT in the columns was calculated directly from the measured void volume (Eq. 1) using the column volume ($V_{columns}$) and wastewater flow rate (Q).

$$HRT = \frac{V_{water}}{V_{sample}} \cdot \frac{V_{reactor}}{Q} = \varphi . \frac{V_{columns}}{Q} \quad (1)$$

The elemental compositions of the materials tested (Table 2) were determined via X-ray Fluorescence (XRF) measurements performed in a Panalytical device (model Axios Max), equipped with an Rh-tube (maximum power of 4 KW), five analyser crystals and four coupled detectors. The elemental compositions were calculated using the Omnian software. The mineralogical composition of the samples was evaluated using X-Ray diffraction analysis (XRD, Fig. S3) measurements (Table 2), utilizing a Rigaku device (smartlab 9 kW, 2015) equipped with a Co X-Ray source (40 kV, 135 mA) and a goniometer with a Bragg-Brentano geometry (300 mm).

Electrical conductivity of the EC materials was analysed by Eurofins (BobritzschHilbersdorf, Germany) following the internal method SAAHLfPflanzenkohle.040, with measurements taken under 1.2 t pressure. Gravel conductivity was measured separately at the University of Tampere (Finland) using a Keithley 6510 and 7510 with voltage sources Keithley 2290E5 and Tenma 7,213,350. Because different analytical methods were used, the gravel and EC material conductivity values are not directly comparable; the gravel measurement serves only to confirm its inertness and negligible conductivity. The surface area of materials was analysed by nitrogen sorption (Micromeritics ASAP 2020), using a 10 °C/min ramp from room temperature to 105 °C and 14 h degassing under vacuum. The BET (Brunauer-Emmett-Teller method) and pore volume calculations were done with the Micromeritics software. The wood pellet biochar had the greatest surface area and pore volumes, followed by the woodchip biochar (Table 2).

Table 2
Materials tested and their general properties, in addition to elemental composition (XRF) as oxides (most abundant >1%) (full data in Supplementary material Table S1).

General properties	Olive pit Biochar	Wood pellet Biochar (Douglas fir)	Woodchip Biochar (Pine)	Coke (Charcoal)	Gravel
EC (mS/cm)	700	47	9.8	1700	7.9E-07
Surface area BET (m^2/g)	21.13	175.06	124.73	21.67	4.29
% particles <11.2 mm	69	87	29	62	40
Bulk porosity (%)	56	64	63	56	51
t-plot micropore volume (cm^3/g)	0.0112	0.0685	0.0493	0.0027	0.0002
Cumulative pore volume P/P^0 = 0.995 (cm^3/g)	0.0026	0.0366	0.0224	0.0452	0.0213

Elemental composition (XRF) Oxide %	Olive pit Biochar	Wood pellet Biochar (Douglas fir)	Woodchip Biochar (Pine)	Coke (Charcoal)	Gravel
C	89.7	95.6	96.7	95.7	0.1
Na_2O	0.0	0.1	0.0	1.2	2.8
MgO	0.1	0.9	0.1	0.1	2.2
Al_2O_3	2.7	0.1	0.0	0.0	13.2
SiO_2	4.5	0.3	1.1	0.2	69.5
SO_3	1.9	0.3	0.0	0.1	0.1
K_2O	0.1	0.8	0.7	0.5	2.6
CaO	0.2	1.3	1.0	1.7	2.0
Fe_2O_3	0.6	0.2	0.0	0.2	6.5
Other	0.3	0.3	0.2	0.2	1.0

Materials' surface characteristics (Fig. S4) were examined using a scanning electron microscope (SEM). SEM images were taken from unused samples of the tested materials. Samples were coated with a conductive carbon coating, and imaging was performed using a Zeiss (Oberkochen, Germany) Ultra Plus field emission scanning electron microscope (FESEM). The morphology of the materials was investigated using secondary electrons at a 5 kV accelerating voltage and a working distance of 5–7 mm. Gravel displayed a solid and relatively smooth surface, whereas the EC materials exhibited high porosity with distinctly textured surfaces. Wood pellet biochar and coke presented the most porous morphologies, characterized by deep, irregular, and unstructured crevices. Olive pit and woodchip biochar also showed textured surfaces, though their surface crevices appeared more superficial. In the case of the woodchip biochar, the surface features were organised into shallow, elongated pores structured in a longitudinal pattern (Fig. S4).

The surface chemistry of the carbon materials was analysed by Xray photoelectron spectroscopy (XPS) using a Thermo Fisher Scientific ESCALAB 250Xi with an Al Kα source (1486.6 e*V*), 650 μm spot size, and CAE mode. Highresolution spectra were collected at 20 eV pass energy with a 0.1 eV step size. Spectral deconvolution was performed in Thermo Avantage (v5.9925) using the Powell algorithm and Gauss–Lorentz product functions. The nature of oxygen surface groups present on the carbon materials was studied by Fourier transform infrared spectroscopy (FTIR). The samples were analysed with a Nicolet iS20 infrared-spectrometer using the ATR-FTIR technique.

2.5. Microbial community analysis

To investigate bacterial biofilm composition on biofilter materials, 15 mL bed samples were collected from each column at the top (0–5 cm), middle (22.5–27.5 cm), and bottom (45–50 cm). MilliQ water with glycerol TE buffer (100 µL per 1 mL water) was added to preserve biofilms. Samples were stored at −20 °C until granule pre-treatment.

2.5.1. DNA extraction and sequencing

As pre-treatment frozen samples were thawed, biofilm detachment was carried out using the vortex-sonication-vortex method (V-S-V) (Sherertz et al., 1990; Oliva et al., 2013) with 30 s vortexing, sonicating for 10 min at 30 kHz (taking breaks every 2 min to rest the sample on ice to prevent heating), and a final 1-min vortexing. Biomass samples were centrifuged at 500 ×*g* for 5 min, then at 14,000 ×g for 5 min to pellet cells. The pellet was resuspended in 600 µL 1 × PBS and split into two 1.5 mL Eppendorf tubes.

The community composition of bacteria was assessed through amplicon sequencing of 16S rRNA genes. From the pre-treated samples, nucleic acids were extracted using a modified phenol extraction protocol (Lim et al., 2016) and RNA was removed by RNase A treatment (Thermo Scientific EN0531) before DNA precipitation. DNA was amplified by PCR with primers 27F (5′-AGAGTTTGATCCTGGCTCAG-3′; Weisburg et al., 1991) and 1492R (5′-GGTTACCTTGTTACGACTT-3′; Weisburg et al., 1991) (Biomers, Germany) using 35 cycles of 95 °C for 44 s, 57 °C for 45 s, and 72 °C for 1 min with pre-incubation at 95 °C for 5 min and a final extension step at 72 °C for 5 min. Barcodes from the Oxford Nanopore PCR barcoding kit 96 (EXP-PBC096) were added in a second PCR: 3 min at 95 °C, then 15 cycles of 95 °C for 30 s, 62 °C for 30 s, 68 °C for 90 s, and 80 °C for 15 s, with a final 5 min at 68 °C. The PCR products were pooled and purified using AmpureXP magnetic beads (Beckman Coulter) according to the manufacturer's protocol. The PCR products were sequenced on an Oxford Nanopore Flongle (R10.4.1) using the Ligation Sequencing kit (SQK-LSK-114) according to the manufacturer's instructions yielding full-length 16S reads. Basecalling was done in Dorado using the Super accurate basecalling model (GitHub - nanoporetech/dorado: Oxford Nanopore's Basecaller).

2.6. Calculations and data analysis methods

2.6.1. Systems performance: load removal

Daily contaminant mass load (Load) to the system was determined using daily flow rates (Q) and the concentrations (Conc) of selected substances (i) measured in samples collected in each sampling event (Eq. 1). Discharge loads were determined similarly, using the measured concentrations in outflow samples. Contaminant load removal efficiency (RE %) was calculated based on the difference between inflow load (L_{in}) and outflow load (L_{out}) (Eq. 2):

$$\text{Load}_i\left(\frac{\text{mg}}{\text{d}}\right) = \text{Q}\left(\frac{\text{L}}{\text{h}}\right)*24\left(\frac{\text{h}}{\text{d}}\right)*\text{Conc}_i\left(\frac{\text{mg}}{\text{L}}\right) \quad (2)$$

$$\text{RE}\ (\%) = \frac{L_{in} - L_{out}}{L_{in}}*100\% \quad (3)$$

A correlation analysis to investigate the relationship between removal efficiency and contaminant load was performed in RStudio (R Core Team, 2022) using Spearman correlations. Analysis of variance (ANOVA) and Tukey's Honest Significant Difference (HSD) test was done in Rstudio (R Core Team, 2022) package 'stats' to see if there was a statistically significant ($p < 0.05$) difference between the different materials or between the flow rates to the columns and to identify which group means in the sets were significantly different from each other. Assumptions of ANOVA were checked using Shapiro–Wilk and Levene's tests, and Welch's ANOVA was applied when variances were unequal. Although Kruskal–Wallis tests on unit-level means had limited statistical power (n = 2–3 units per material, Table S2), they showed the same ranking and direction of material performance as the ANOVA. This indicates that the observed differences are robust despite the unbalanced replication. Effect sizes were calculated using partial η^2 (with 95% confidence interval (CI)) and Cohen's d; full results are provided in the Supplementary Material (Table S3).

2.6.2. Gas flux estimation

To estimate the flux of CH_4, CO_2, and N_2O emitted by the systems, gas mass emissions rates were determined from the chamber measurements by plotting Ci (gas concentration in g/m^3 obtained by Eq. 3) against time t (in days). In Eq. 3, Conc_i is the concentration of a gas in ppm, R is the gas constant (0.000082057 atm·m^3/mol·K), T is the absolute temperature (K), and P is the absolute pressure of the gas (atm). The slope (m) from a linear fit of the data (Ci x t) gives the mass emissions rate (mg/m^{3}d). Subsequently, the mass emission rate was used to compute the emissions per area using Eq. 4, where Vc is the volume of the collection chamber (m^3), and Asc is the surface area of the chamber (m^2). Total GHG flux was defined as the sum of CO_2, CH_4, and N_2O fluxes, and each gas's percentage was calculated as its proportional contribution to this total.

$$\text{Ci}\left(\frac{\text{mg}}{m^3}\right) = \frac{\text{Conci}\ \frac{(ppm)}{10^6}*\text{MW}\left(\frac{\text{g}}{\text{mol}}\right)*\left(\frac{1000\ \text{mg}}{1\ \text{g}}\right)}{\frac{RT}{P}} \quad (4)$$

$$\text{Flux}\left(\frac{\text{mg}}{m^2}\right) = \text{m}\left(\frac{mg}{m^3 d}\right)*\frac{Vc\ (m^3)}{\text{Asc}(m^2)} \quad (5)$$

2.6.3. Microbial community bioinformatics

Sequenced data were processed in QIIME2 (v2024.5.0; Bolyen et al., 2019). Sequences were trimmed with cutadapt (Martin, 2011) by discarding reads lacking a forward primer and retaining those ≥1000 bp without a reverse primer. Dereplication was performed with vsearch (Rognes et al., 2016), and forward sequences were oriented using rescript (Robeson et al., 2021). Forward and reverse sequences and tables were merged with the feature-table plugin, and taxonomic classification was conducted using the feature-classifier plugin (Bokulich et al., 2018) against the SILVA 138 reference database at a confidence threshold of 0.7.

Unassigned and Domain-only taxa were removed due to suspected low sequencing quality. The dataset was rarefied to an even depth of 1048 sequences, corresponding to the lowest sample depth. Rarefied data were used for community composition plots (Supplementary material), and non-rarefied data for relative abundance plots. To assess the sensitivity of rarefaction, we repeated the rarefaction procedure 10 times using different random seeds. Across all runs, the global top 10 genera were identical, and the resulting community patterns were highly consistent with those obtained from the non-rarefied relative abundance. Visualization and downstream analyses were conducted in R (v4.2.1; R Core Team, 2022) using MicroViz (Barnett et al., 2021) for taxa selection, MicEco (Russel, 2024) for Venn diagrams, and ComplexHeatmap (Gu et al., 2016) for heatmap generation. The EAB were identified using the list reported by Garbini et al. (2023), while nitrifiers and anammox bacteria were identified using lists from Ge et al. (2015) and Xia et al. (2019). Detailed plugin versions, parameters, and the full R package environment are provided in Supplementary material (Table S4).

3. Results and discussion

3.1. Treatment efficiency and the influence of incoming load

3.1.1. Systems performance

Overall, columns filled with EC materials achieved greater removal of COD and N fractions across the 32-week experimental period when compared to gravel, despite minor fluctuations in the final weeks

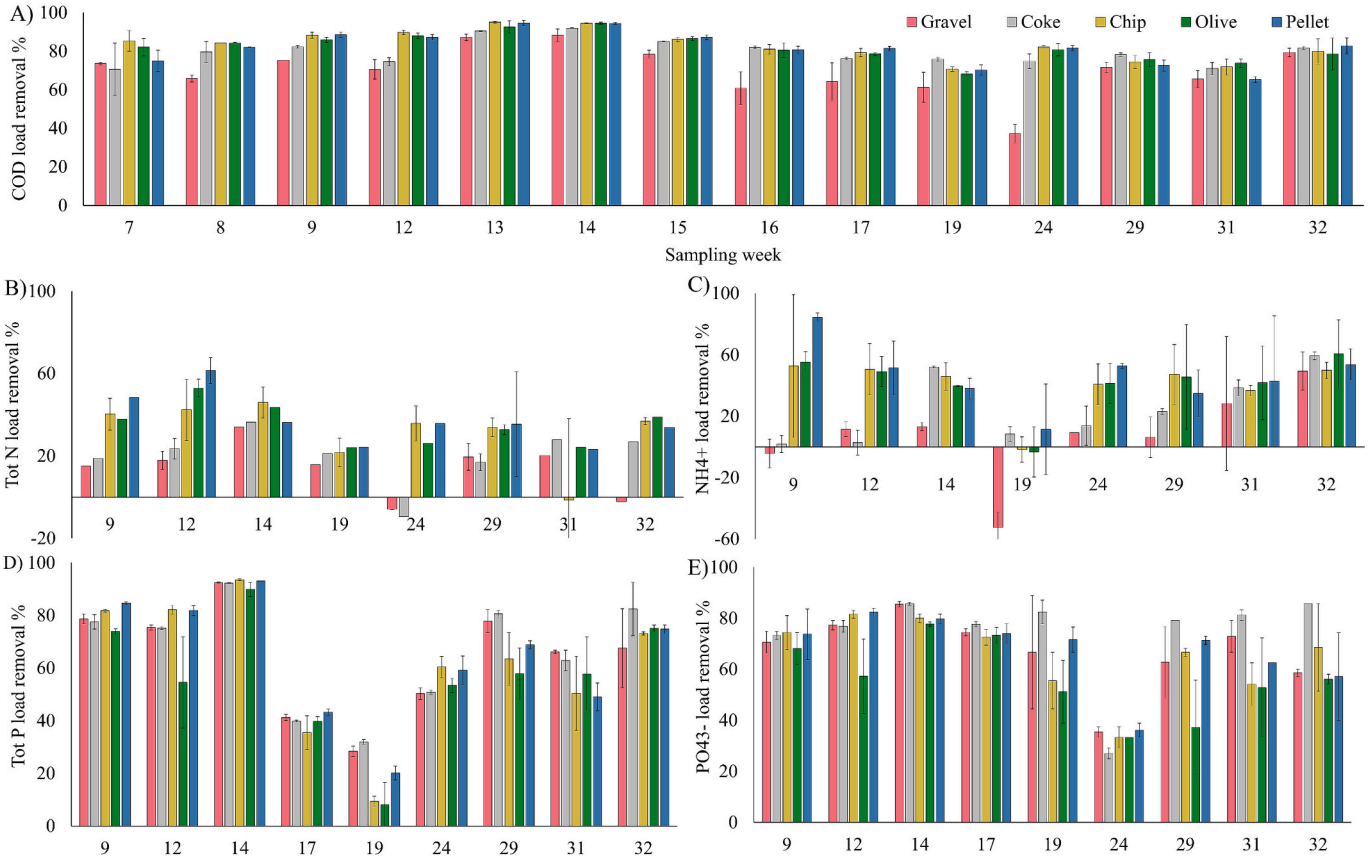

Fig. 2. Average load (mg/d) removal efficiency (%): A) COD, B) Total nitrogen (Tot N), C) ammonium (NH_4^+—N), D) Total phosphorus (Tot-P), and E) phosphate (PO_4^{3-}-P). The X-axis represents operation weeks, and the error bars represent the difference between average load removal and the minimum and maximum load removal values. Nitrogen and phosphorus fractions were analysed from selected samples (ca 65% of all events) due to cost and equipment availability restrictions.

(Fig. 2). Among the EC materials, coke columns removed more P on average, while the biochar systems were better at removing COD and N. Wood pellet biochar columns achieved the highest removal rates but also the largest fluctuations in performance. The removal of organics varied during the experiment, but the variation was low within replicated systems of the same material in individual sampling events. On the other hand, significant variations, both among sampling events and system replicates, were observed for the removal of N and P, especially for NH_4-N and PO_4-P fractions (Fig. 2). These larger fluctuations in N and P removal also reflect occasional negative removal efficiencies, which can arise from analytical uncertainty, biofilm washout, or internal nitrogen transformations such as mineralisation.

Overall, satisfactory COD load removal efficiency was achieved across all materials. Woodchip biochar-filled columns attained the highest average removal efficiency (83.0% ± 7.6), followed closely by olive pit biochar (82.1% ± 7.2), wood pellet biochar (81.7% ± 8.6), coke (79.6% ± 6.5), and gravel (69.7% ± 12.8) (Table S5). Effluents from electroconductive (EC) materials met the <125 mg/L COD requirement in 93% of sampling events for coke and in 100% of events for all biochar materials, whereas gravel-filled systems met the limit in only 79% of events. Statistical analysis (ANOVA with Tukey's post-hoc tests, $p < 0.05$) confirmed that gravel's removal efficiency was significantly lower than that of all other materials (Table S5). Biochar materials achieved significantly higher mean COD removal than gravel, but their performance was not statistically different from coke. These patterns were supported by effect-size analysis: Material explained 20% of the variance in COD removal (partial $\eta^2 = 0.20$; 95% CI, Table S3), and pairwise effect sizes showed large differences between gravel and all EC materials (Cohen's d = 0.89–1.26, 95% CI: 0.33–1.79). Differences between biochar materials and coke were small and non-significant for COD (d = 0.25–0.44, 95% CI overlapping zero), but moderate to large and statistically significant for TotN and NH_4 (d = 0.61–1.25, 95% CIs excluding zero), while differences among biochar materials remained small and non-significant (Table S3). These findings are consistent with prior research (Peñacoba-Antona et al., 2022; Prado et al., 2019; Prado de Nicolás et al., 2022), which, although limited, consistently reports that electroconductive materials outperform gravel in terms of COD removal in MET systems. Additionally, EC biochars tend to perform better than materials with higher electric conductivity, such as graphite and coke (Prado et al., 2019; Prado de Nicolás et al., 2022). Volumetric removal rates ranged from 33 to 65 g COD/m^3·day for biochar materials, compared to 18–44 g COD/m^3·day for gravel. These values fall within the ranges reported in previous MET-focused studies (Prado et al., 2019), which observed 31–137 g COD/m^3·day at inflow concentrations of 170–890 mg/L (this study: 138–800 mg/L).

The removal of tot-N was generally low, consistent with findings from other studies on fully saturated systems (Koukoura et al., 2024), where anaerobic conditions have been linked to reduced performance. Among the tested materials, wood pellet biochar achieved the highest average tot-N removal (37.1% ± 14.3), followed by olive pit biochar (35.2% ± 15.2), woodchip biochar (33.9% ± 39.5), coke (22.0% ± 31.6), and gravel (16.7% ± 23) (Table S5). Patterns of ammonium (NH_4-N) removal closely mirrored those of tot-N (Fig. 2B,C). However, NH_4-N removal rates were generally higher than those for tot-N. Maximum removal efficiencies reached 84.4% for biochar materials and 49.4% for gravel. For tot-N, the highest removal rates were 61.5% for biochar and 39.6% for gravel. Statistical analysis confirmed that biochar achieved significantly higher mean NH_4-N removal compared to coke and gravel, with the strongest difference observed between biochar and gravel (Table S6, Supplementary material). Prado de Nicolás et al. (2022) have

presented supporting results as they also identified significant differences in ammonium removal between biochar, coke, and gravel.

The removal of total nitrogen achieved per volume of bed material was on average 4.3 g Tot N/m^3day for the three biochar materials, higher than the removal achieved by gravel, which was on average 2.2 g Tot N/m^3day. The removal observed for biochar materials was higher than values reported in the Peñacoba-Antona et al. (2022) MET-focused study, which had a removal of 2 g Tot N/m^3day with similar inflow concentrations of TN between 40 and 70 mg/L.

Regarding the material properties that may support the better performance of EC-materials, beyond electrical conductivity, physicochemical properties also play a key role in microbial-driven processes. Prado et al. (2019) highlighted that porosity and surface chemistry influence bacteria-to-material electron transfer. The best-performing materials for nutrient and COD removal, wood pellet and woodchip biochar, had the lowest EC and the highest surface area, bulk porosity, microporosity volume, and the most porous textured surface morphology (Table 2). Such characteristics provide abundant attachment sites for biofilm growth and are consistent with the hypothesis that they may enhance system efficiency (Baek et al., 2021; Prado et al., 2019). Greater surface area also increases contact between biofilm, pollutants, and the material, which may further improve removal. However, in wood pellet and woodchip biochar, approximately 50% of pore volume consisted of micropores, which may be prone to blockage by, for example, biofilm growth (Saeed et al., 2020).

Aiming to investigate how surface chemistry may have affected biofilm diversity and contributed to the different materials' performances, FTIR and XPS analyses were conducted. FTIR spectra of EC materials exhibited weak absorption features and a rising baseline in the 4000 to 400 cm^{-1} wavenumber regions, typical of carbon-rich, highly absorbing samples that have been treated at high temperatures. Wood pellet and woodchip biochar displayed slightly more structure than the other carbonaceous materials, but the signals remained too weak for reliable functional group identification. The O 1 s XPS spectra (Fig. S5) clearly distinguish the inorganic gravel from the carbon-based EC materials. Gravel's observations are consistent with the XRD results (Fig. S3). The EC materials showed higher binding energies due to overlapping contributions from different organic groups, like C═O (~531–532 eV) and C—O (~533–534 eV) (Zhao et al., 2018). Coke and olivepit biochar exhibited broad bands spanning 529–535 eV, with the olivepit biochar showing relatively greater intensity at lower binding energies. Wood-derived biochars displayed broad features between 530 and 534 eV, with the woodchip biochar showing higher contributions at the higher binding energies. These patterns suggest higher proportions of C=O-rich groups (e.g., ketones, lactones, carboxyls) in coke and olivepit biochar, and more C–O-rich groups (e.g., alcohols, ethers, hydroxyls) in the wood-derived materials. Overall, although the analyses conducted suggest that the EC materials have more diverse oxygen-containing surface features than gravel, they did not provide precise quantification or definitive identification of functional surface groups, and therefore, no conclusive remarks can be made regarding the effect of surface chemistry on the materials' performance.

Beyond microbiologically driven processes, studies not focusing on MET systems, but which tested biochar as media in vertical flow CW, have also reported higher contaminant removal (e.g., COD and other organic compounds, NH_4-N, etc.) in biochar systems when compared to inorganic materials such as gravel (Vymazal et al., 2021; Panghal et al., 2025). The higher removal rates have been linked to higher sorption capacity of biochar, as well as higher abundance of denitrifiers and EAB, such as *Geobacter* in the biofilms developed (Saeed et al., 2020; Panghal et al., 2025). While the approach used in this study does not allow for the distinction between removal processes, it is safe to assume that physical-chemical mechanisms played a role in the performance of both biochar and coke materials.

Based on the organic load introduced to the systems (up to 95 g COD/m^2day) and the removal observed (> 80%), and assuming a person equivalent (PE) load of 100 g COD/day, a surface area of ca 1 m^2 per person equivalent (PE) would be sufficient for MET systems operating at a HRT between 3 and 4 days to meet COD discharge requirements. However, caution should be exercised when extrapolating findings from small pilot-scale experiments, such as those conducted here, to full-scale systems. Additional research at representative operational scales is required to substantiate the emerging evidence that MET systems may require less surface area than conventional constructed wetlands (Vymazal et al., 2021; Vymazal, 2023). The cost of materials is an important factor for media selection. A straightforward cost comparison of the materials tested shows that locally the gravel used costs approximately 70 €/t, whereas the biochar materials and coke are around 22- and 29-times more expensive, respectively. Although biochar products are considerably more expensive than gravel, they remain cheaper than coke, and the reduced footprint of MET systems means that less material is required overall.

3.1.2. Correlation between incoming load and load removal

Although the hydraulic load was maintained constant, the mass load varied over the experimental period due to fluctuations in wastewater quality at the treatment plant. Across individual sampling events, no statistically significant differences in inflow mass loads were observed among columns, confirming that systems packed with different materials received homogeneous inputs (Table S7). Most materials exhibited statistically significant positive correlations between COD load and COD removal efficiency, ranging from moderate to strong (0.65–0.95). This indicates that higher COD loads were associated with enhanced removal performance (Table 3). Biochar-based materials showed the strongest correlations, suggesting that these materials may offer greater degradation capacity for organic matter under higher loading conditions. A similarly positive correlation between load and removal rates in MET systems has been reported elsewhere (Peñacoba-Antona et al., 2022; Prado et al., 2019; Prado de Nicolás et al., 2022), with the difference in performance between gravel and EC materials increasing with increasing load.

Changes in organic loading (COD) had a stronger influence on Tot-N

Table 3
Correlation coefficients obtained for the relationship between inflow COD load (mg/d) and COD, tot-N, and tot-P removal efficiency. In addition to correlations between inflow tot-N load (mg/d) and tot-N removal efficiency, tot-P load (mg/d) and tot-P removal efficiency, and PO_4^{3-}-P load (mg/d) and PO_4^{3-}-P removal efficiency. Only statistically significant correlations ($p < 0.05$) are presented.

Material	Correlation COD load			Correlation tot-N load	Correlation tot-P load	Correlation PO_4^{3-}-P load
	COD	Tot-P	Tot-N	Tot-N	Tot-P	PO_4^{3-}-P
Gravel R1					0.7	0.62
Gravel R2	0.65				0.7	
Coke R1						
Coke R2					0.72	
Woodchip R1	0.9				0.87	0.72
Woodchip R2	0.77	0.66	0.66		0.87	0.71
Woodchip R3	0.91	0.73	0.84		0.95	0.65
Olive Pit R1	0.9		0.66		0.63	0.75
Olive Pit R2	0.82		0.68		0.7	0.7
Olive Pit R3	0.95		0.71		0.67	0.67
Wood Pellet R1	0.77	0.69			0.92	0.72
Wood Pellet R2	0.87	0.83	0.87	0.77	0.93	
Wood Pellet R3	0.86	0.77	0.68		0.91	

removal than on Tot-P. Correlations between COD load and Tot-P removal were moderate and inconsistent across materials and replicates, indicating only limited indirect effects. In contrast, moderate to strong correlations between COD load and Tot-N removal (0.66–0.87) were observed for biochar-filled pilots. This suggests that higher organic loading may be linked to enhanced denitrification, potentially through increased carbon availability. However, correlations between total N load and Tot-N removal were generally not significant (Table 3), reflecting the complexity of nitrogen transformation processes such as nitrification and denitrification, which depend more on redox conditions, microbial activity, and carbon availability than on loading alone. For phosphorus, correlations between total-P or PO_4^{3-} load and removal were stronger (0.63–0.72), indicating that P removal was more directly influenced by P loading, most likely through adsorption or precipitation mechanisms.

3.1.3. Micropollutant removal

Of the 120 substances analysed, 74 were detected in the inflowing wastewater, with the contrast agent Iomeprol (45,600 ng/L) and the antiepileptic Gabapentin (30,600 ng/L) showing the highest concentrations (Table S8). Removal was generally higher in electroconductive (EC) material-filled columns (Table 4), with woodchip biochar achieving the highest efficiencies for most compounds (e.g., >90% for Benzotriazole and Metoprolol), followed by wood pellet and olive pit biochar systems. Micropollutant (MP) removal in these systems depends not only on the physicochemical properties of the substances (e.g., hydrophobicity, aromaticity, ionisation) but also on the characteristics of the media, which influence sorption and microbial degradation through effects on biofilm development and activity (Pun et al., 2019; Bhat et al., 2024). The results align with Pun et al. (2019), who reported higher pharmaceutical removal in MET systems compared to conventional constructed wetlands (CW).

Regarding the processes that might have influenced MPs' retention in the EC material-filled columns, the restricted data set did not provide any consistent pattern which could be used to link measured values to specific processes or mechanisms. In general, sorption in biochar systems is often considered an important pathway (Pun et al., 2019); however, compounds with higher Log Kow values (e.g., diclofenac, carbamazepine, venlafaxine) showed varying removal across biochar-filled columns, with no consistent relationship between hydrophobicity and removal rates (Table 4). Similarly, MPs removal in the wood pellet biochar columns, despite their large surface area, was lower than in other biochar systems. Biodegradation is another possible contributor, as MET systems have been associated with enhanced microbial extracellular electron transfer (Prado et al., 2019; Zhang et al., 2023), and the higher COD removal and redox conditions in EC systems are consistent with this possibility. That said, the data produced does not allow the distinction among these potential mechanisms. Therefore, the results reported should be considered exploratory, as they represent a snapshot rather than evidence of possible removal mechanisms or performance.

3.2. Gas emissions and microbial community analysis

3.2.1. Gas flux measurements

Gas emissions varied between monitoring events, material type, and between replicated systems of the same material (Fig. 3A-3C). In general, emissions were higher during the first week of measurement (week 22), despite both organic and nitrogen load and removal being lower during this period (Fig. 3E and F). Biochar-filled columns on average produced higher carbon dioxide (CO_2) fluxes compared to gravel and coke, with gravel showing the lowest concentrations (Fig. 3B). Woodchip biochar columns exhibited the highest methane (CH_4) emissions (Fig. 3A). In contrast, wood pellet biochar columns showed the highest nitrous oxide (N_2O) fluxes (Fig. 3C). To the authors' knowledge, no prior reports exist on GHG emissions from MET systems. However, studies on microbial fuel cells (MFCs) and MFC-constructed wetlands (Wang et al., 2019; Wang et al., 2024; Xu et al., 2021) suggest that GHG emissions from MFCs may be lower than those from conventional constructed wetlands, likely due to competition between methanogens and EAB, which can suppress CH_4 production (Zhang et al., 2023). MFC-constructed wetlands provide the closest available context for GHG emissions in MET systems, although these systems differ substantially from the studied systems in hydraulics, media, plant presence, and the use of an external circuit.

Based on the measurements conducted, biochar columns had higher fluxes of CO_2 and N_2O and, in most cases, more CH_4 than gravel and coke columns. Higher CO_2 and N_2O amounts may indicate higher microbial activity in those columns (Yu et al., 2010). This pattern aligns with the higher removal of organic matter and N observed in biochar columns (Fig. 3), although causality cannot be established. Porewater sampling showed that most organic matter (COD) was removed in the bottom layers of the columns (Fig. S6), consistent with anaerobic carbon removal. Anaerobic digestion typically produces biogas with 50–70% CH_4 and 30–50% CO_2 when no alternative electron acceptors are present (Okopi et al., 2024). In contrast, the studied systems were dominated by CO_2 (98.5 ± 0.5%), with CH_4 at 0.9 ± 0.5% and N_2O at 0.7 ± 0.1%, which indicates a dominant aerobic degradation.

Nitrogen transformation patterns further support this interpretation. The ratio of N_2O-N to total N removed was low (average 0.04; Table S9), indicating that most nitrogen was converted to N_2 rather than N_2O. Processes such as denitrification, dissimilatory nitrate reduction to ammonia, aerobic ammonia oxidation, and nitrification are all associated with N_2O production (Xu et al., 2024; Yu et al., 2010). In this study,

Table 4
Average ($n = 3$ (biochars) and $n = 2$ (coke and gravel) replicates) micropollutant removal efficiency. Negative values indicate net release/leaching/formation of the substance, while ± values represent the variation to the maximum and minimum removal rates among the n replicates. Selected compounds based on EU regulations, full data in Table S8. One compound (2-hydroxycarbamazepine) was below the detection limit in the woodchip outflow sample; in this case, DL/2 was used for removal-efficiency calculations.

	Removal %				
Substance	Gravel	Coke	Olive pit	Woodchip	Wood pellet
1-H-Benzotriazole	−25.2 ± 11.5	85.1 ± 0.1	90.5 ± 3.6	97.9 ± 1.5	74.5 ± 8.1
5-Methyl-1-H-benzotriazole	−8.1 ± 11.1	63.5 ± 1.3	87.1 ± 2.2	93.2 ± 1.3	59.5 ± 3.0
Carbamazepine	−28.5 ± 4.6	41.6 ± 9.7	53.5 ± 2.9	64.4 ± 9.7	9.6 ± 0.4
2-Hydroxycarbamazepine	−85.0 ± 23.6	13.8 ± 0.0	5.7 ± 1.1	59.4 ± 0.0	−67.1 ± 0.6
10,11-dihydro-10-hydroxycarbamazepine	19.3 ± 62.2	19.3 ± 18.6	76.9 ± 31.8	77.7 ± 18.6	79.9 ± 26.8
Diclofenac	−6.9 ± 6.3	60.4 ± 9.4	30.3 ± 10.6	53.4 ± 9.4	8.8 ± 8.9
4'-Hydroxydiclofenac	18.0 ± 21.9	60.6 ± 17.0	16.3 ± 39.1	54.9 ± 17.0	18.7 ± 34.5
Hydrochlorothiazide	−31.5 ± 21.0	34.9 ± 16.5	50.4 ± 2.9	53.1 ± 16.5	1.0 ± 17.4
Metoprolol	−10.9 ± 2.7	74.1 ± 3.7	90.0 ± 1.2	92.1 ± 3.7	76.1 ± 6.6
Venlafaxine	30.4 ± 12.4	53.4 ± 4.9	70.7 ± 7.5	86.1 ± 4.9	69.7 ± 2.1
O-Desmethyl venlafaxine	0.9 ± 7.6	−11.7 ± 12.2	32.1 ± 5.9	52.9 ± 12.2	31.3 ± 11.5

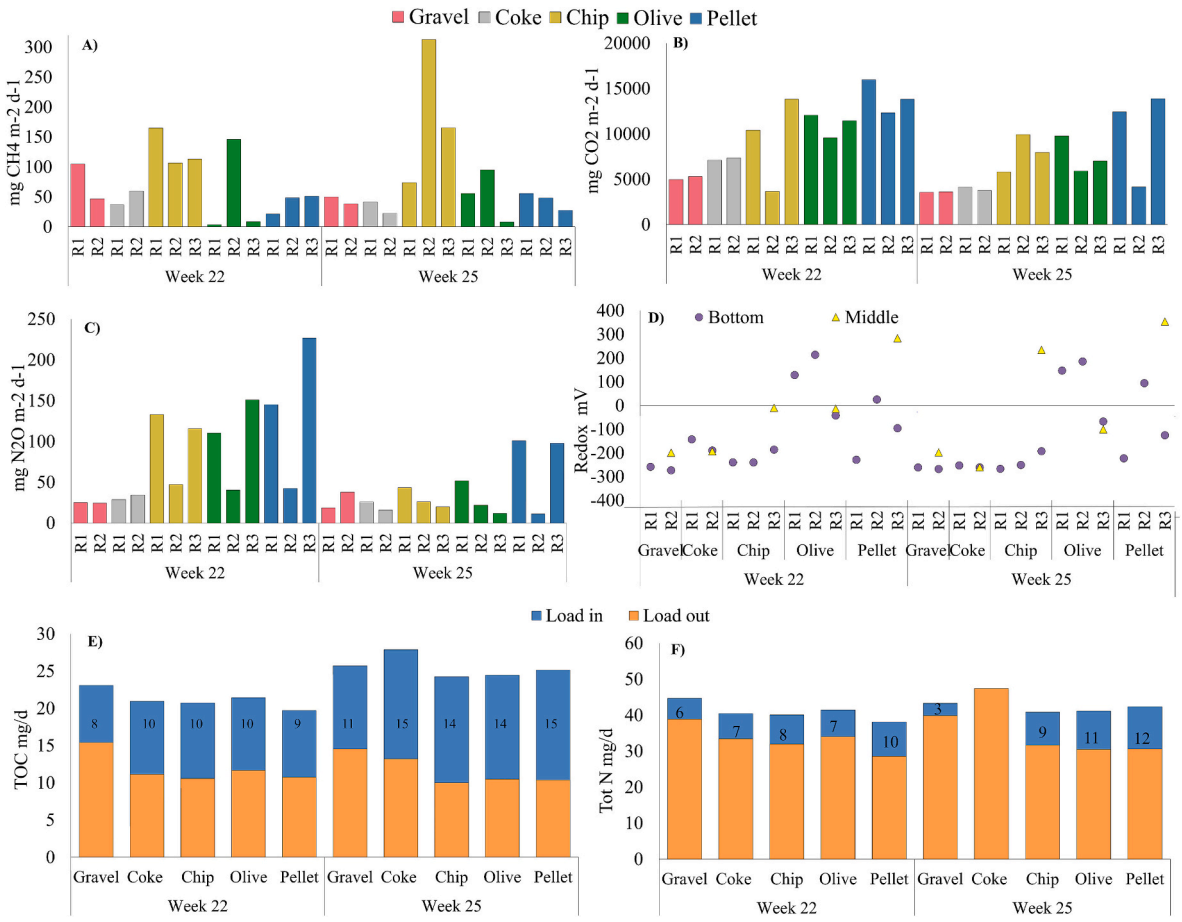

Fig. 3. Gas emissions for each material and replicated system (A-C), redox measurements during gas sampling days (*D*), and inflow and outflow daily load with load removal provided as values inside the bars (*E*-F). Replicate columns of the same material are referred to as R1, R2, or R3.

porewater analyses showed that NH_4^+ and total nitrogen removal occurred mainly in the top layer (Fig. S6), consistent with elevated NO_3^- concentrations in column outflows. Some NH_4^+ removal also occurred at the column bottoms, although gravel systems exhibited negative removal and wood pellet systems occasionally showed slightly negative values. Low inflow NO_3^- concentrations (Table 2) suggest that denitrification in the anoxic bottom layers was limited, making it unlikely to explain the higher N_2O emissions and nitrogen removal observed in biochar columns.

In conventional wetlands, oxic upper layers and anoxic lower layers establish redox gradients that influence pollutant removal (Aguirre et al., 2005). Similarly, in METs, oxygen availability enhances electron flow and removal efficiency (Prado et al., 2020). In this study, biochar columns had significantly higher effluent dissolved oxygen (DO) than gravel and coke (Table S6). Elevated effluent DO indicates that the outflow region of the biochar columns remained more oxidative, potentially creating conditions favourable for aerobic processes such as nitrification, where NH_4^+ is oxidized to NO_2^- and NO_3^- with N_2O as byproducts. Biochar systems also showed greater COD and NH_4^+ removal and higher NO_3^- accumulation, which is compatible with this interpretation but not sufficient to confirm specific pathways.

All columns showed lower redox potential at the bottom compared to the middle, indicating more reducing conditions at the bottom where wastewater was introduced to the columns (Fig. 3D). In coke- and gravel-filled systems, the gradient was minimal, with negative values even at the middle section. In contrast, wood pellet and woodchip biochar columns exhibited a pronounced vertical redox gradient with very reduced conditions at the bottom and strong oxidative conditions at the top (Fig. 3D). Systems with more stable, negative redox at the bottom and the highest positive redox at the surface typically have the greatest potential for EAB activity (Doherty et al., 2015; Prado et al., 2019). Across weeks, variation in redox potential was minor (Fig. S2), and no clear correlation with GHG emission rates was observed (Fig. 3).

Mitigation of GHG emissions is an important aspect for wastewater treatment systems. For vertical flow CW, suggested mitigation measures include, among others, optimisation of hydraulic loading rate, effluent recirculation, introduction of active aeration, optimisation of C/N ratio in influents, etc. (Zhang et al., 2026). While no reports are available on GHG emissions from MET systems, such measures, when optimised for the specific type of systems, can be expected to also abate CH_4 and N_2O emissions.

3.2.2. *Microbial community analysis*

Bacterial communities across the different carrier materials shared a set of common genera, with 96 genera (19% of the 438 detected genera) present in all materials based on rarefied genus-level data (Fig. S7). The most abundant genera across materials and depths were *Candidatus Omnitrophus* (phylum Verrucomicrobiota) and *Lentilactobacillus* (family Lactobacillaceae) (Fig. S8). A broader overview of the core microbiota is shown in the heatmap (Fig. 4C), where lactic acid bacteria (LAB) accounted for 25% of the core community. Biochar materials were distinguished by higher relative abundances of *Candidatus Omnitrophus*, *Nitrosomonadaceae Ellin6067,* and *Christensenellaceae*, whereas inert gravel supported greater proportions of fermentative LAB, for example, *Pediococcus* and *Lentilactobacillus* (Fig. 4C).

Members of the family *Nitrosomonadaceae,* including *Nitrosomonas* and *Nitrosospira*, are commonly found in wastewater treatment environments and function as aerobic chemolithoautotrophic ammonia

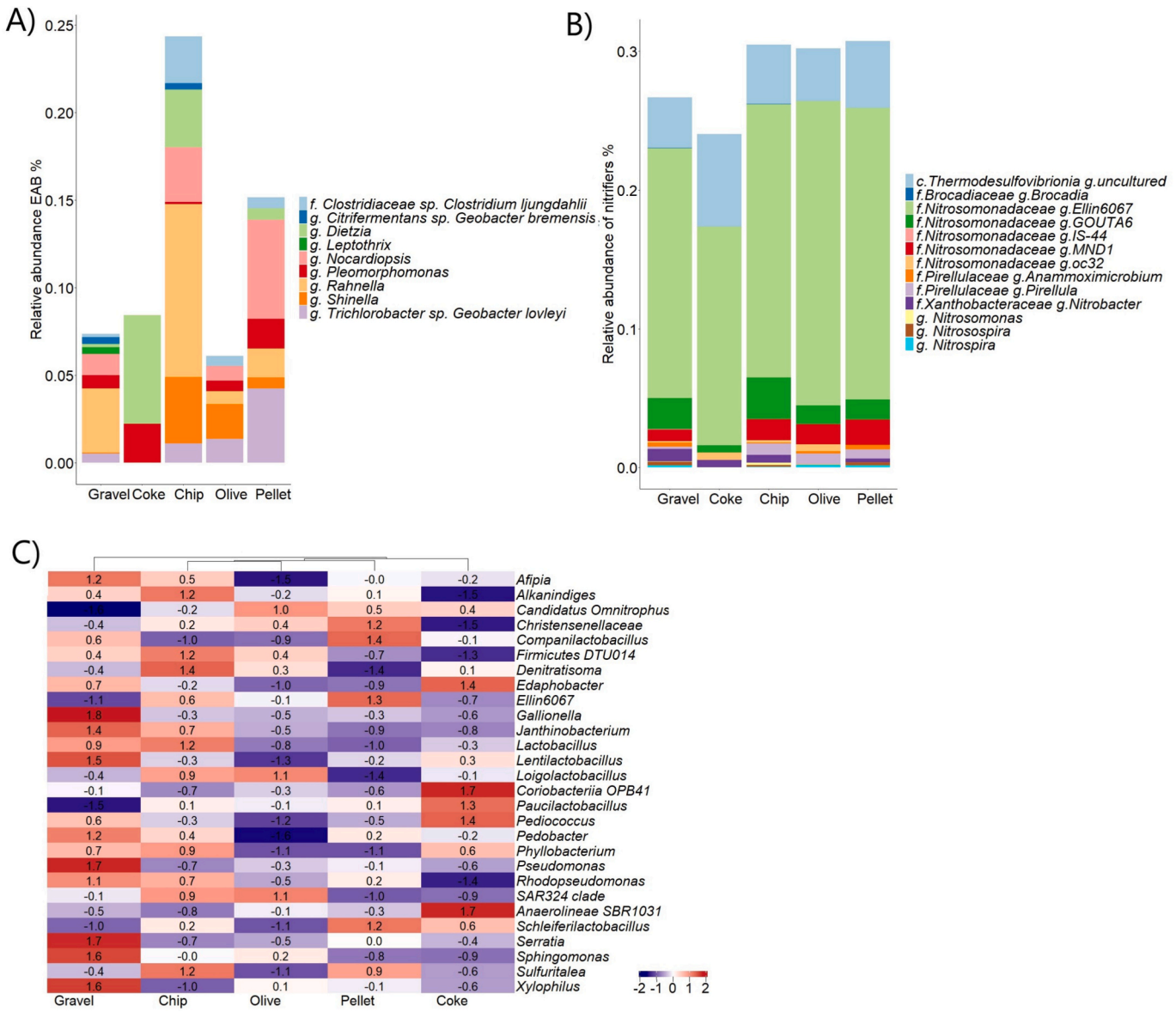

Fig. 4. A) Bar plot of EAB bacteria, B) Relative abundance of nitrifier bacteria in the material, and C) Heatmap of the community composition of core taxa with differential bacterial abundance at genus levels between high (above median) and low (below median) of the core microbiota (detection = 0.001 and prevalence = 0.75).

oxidizers. The class *Thermodesulfovibrionia* comprises obligate anaerobes capable of hydrogen oxidation, sulfate reduction, and, in some cases, nitrate reduction. Together with families *Pirellulaceae* and *Xanthobacteraceae*, these groups were identified as potential nitrifiers in the pilot systems. Their relative abundance was higher in electroconductive (EC) materials compared to gravel biofilms. Within the columns, the most abundant nitrifier was *Ellin6067* (*Gammaproteobacteria*), followed by uncultured *Thermodesulfovibrionia* taxa (Fig. 4B). Higher amounts of nitrifiers in EC materials may explain the higher ammonium removal in these systems.

Furthermore, so-called nitrifier-driven denitrification can occur in aerobic conditions. Genus *Denitratisoma* was identified from the column's core microbiota; bacteria from this genus are known to reduce nitrate to N_2 under aerobic conditions by using nitrate as a terminal electron acceptor (Xia et al., 2019). Differing from the coke and gravel, the biochar materials had a higher abundance of bacteria genera *Pirellula* and *Candidatus Anammoximicrobium* from the bacteria class *Planctomycetes*. Interestingly, the genera *Pirellula* and *Candidatus* Anammoximicrobium are associated with anaerobic ammonium oxidation (anammox) (Khramenkov et al., 2013; Xia et al., 2019). The higher abundance of these bacteria may explain the greater removal of ammonium and total nitrogen in the MET systems. Similarly, higher amounts of anammox-related bacteria were found by Prado de Nicolás et al. (2022).

Electroactive biofilms oxidize organic matter, resulting in the production of electrons, protons, and CO_2. EAB are capable of donating electrons obtained from the oxidation of organic matter to the electroconductive (EC) bed material, which serves as an unlimited electron acceptor. In natural environments, the lack of suitable electron acceptors can slow down degradation processes. However, systems with unlimited electron acceptors should not face this limitation, allowing EAB to make degradation more efficient. The EABs were the most abundant in woodchip biochar-filled columns, while the lowest relative abundance of EAB was in gravel and olive pit biochar columns (Fig. 4A). However, the relative abundance of EABs remained low across all samples. A plausible explanation for the low apparent abundance is the current limitation of EAB reference databases and the mismatch between taxonomy and function within these groups. EABs encompass

organisms from multiple domains and include taxa with diverse and sometimes poorly resolved functional roles, which complicates their detection and classification. In addition, community composition can vary substantially across systems due to environmental and operational differences, meaning that taxa enriched in one engineered environment may not be equally represented in another (Agudelo-Escobar and Cabrera, 2024).

3.3. Overall aspects of experimental approach, findings, and limitations

By combining pilot-scale operation, multi-material comparison, microbial community profiling, and gas flux measurements, this study provides additional evidence supporting the potential of MET systems for wastewater treatment, particularly regarding the removal of organic matter and nutrients. It also offers new insights into the suitability of biochar produced from different biomass sources as MET systems media. Although the results are promising, they should be interpreted with caution. As with any pilot-scale investigation, the scalability of these findings to full-scale MET systems remains uncertain and requires further validation. The assessment of MP removal and GHG emissions was based on only a limited number of monitoring events, restricting the interpretation of the observed gas flux patterns. Similarly, the mechanisms and extent of MP removal could not be fully evaluated due to the limited dataset. A further methodological limitation is the absence of electrochemical measurements, which would have provided valuable context regarding redox behaviour within the system. Future research should therefore incorporate more comprehensive gas flux monitoring, expanded MP sampling campaigns, and dedicated evaluations of scalability across different media materials.

4. Conclusion

This study provides evidence that electroconductive biochars derived from waste biomass can serve as efficient and sustainable alternatives to coke in MET systems. Under identical conditions, biochar-filled columns achieved the highest COD removals (81–83%, with woodchip biochar performing best), followed by coke (79.6%) and gravel (69.7%). Total nitrogen removal showed a similar pattern, with biochars reaching 32.5–34.4%, compared with 21.1% for coke and 13.6% for gravel. Removal efficiencies for COD, total nitrogen, were strongly and positively correlated with daily inflow COD load for biochar materials, indicating that higher organic loading may enhance treatment performance. Biochar-filled columns exhibited higher CO_2 and N_2O fluxes, and in some instances higher CH_4, than gravel and coke, likely reflecting the higher organic and nitrogen removal rates achieved in those systems. Although the overall relative abundance of EAB remained low, they were most enriched in biofilms from the best-performing biochar, suggesting that material properties and microbial composition jointly influence treatment outcomes.

Overall, the findings highlight the potential of biomass-derived electroconductive materials to advance MET systems technology toward more sustainable, circular, and high-performance wastewater treatment solutions. However, although the results are promising, the limitations of the experimental approach must be recognised. The investigations regarding micropollutant removal and GHG emissions were limited in scope, and further research is required to better understand the climate impacts and micropollutant removal capabilities of MET systems. Furthermore, in general, the scalability of pilot-scale findings to full-scale MET systems has yet to be demonstrated.

CRediT authorship contribution statement

Laura Tarvainen: Writing – review & editing, Writing – original draft, Visualization, Methodology, Investigation, Formal analysis. **Katharina Kujala:** Writing – review & editing, Supervision, Methodology, Conceptualization. **Hellen Silva Santos:** Writing – review & editing, Resources, Methodology, Investigation, Formal analysis. **Maarit Liimatainen:** Resources, Methodology. **Elisangela Heiderscheidt:** Writing – review & editing, Writing – original draft, Supervision, Methodology, Funding acquisition, Conceptualization.

Declaration of competing interest

The authors declare that they have no known competing financial interests or personal relationships that could have appeared to influence the work reported in this paper.

Acknowledgements

The study was directly supported by the project “The Future of Nature-Based Wastewater Treatment Solutions: Hybrid Microbial Electrochemical Technology Constructed Wetland (HyMETland, 2021-2026)”, funded by Maa ja vesitekniikan tuki and Kvantum Institute, University of Oulu via the emerging project program. The co-author, Santos, H.S., acknowledges the financial support from the Research Council of Finland (funding decision 347183), and Tarvainen, L., acknowledges the support of the Tauno Tönning Foundation in the form of a personal grant. The authors would like to highlight the help received from representatives from Carbo Culture Oy in the form of material provision and knowledge, and Dr. Carlos Alberto Arias, Aarhus University, in the form of methodology input. The authors would also like to acknowledge the support received from Joni Koivula, laboratory technician at the Water Energy and Environmental Engineering research units, University of Oulu.

Appendix A. Supplementary data

Supplementary data to this article can be found online at https://doi.org/10.1016/j.biteb.2026.102746.

Data availability

Data will be made available on request.

References

Agudelo-Escobar, L.M., Cabrera, S.E., 2024. Microorganisms and Microbial Communities in Bioelectrochemical Systems for Wastewater Bioremediation and Energy Generation. https://doi.org/10.5772/intechopen.112470.

Aguirre, P., Ojeda, E., García, J., Barragán, J., Mujeriego, R., 2005. Effect of Water Depth on the Removal of Organic Matter in Horizontal Subsurface Flow Constructed Wetlands. J. Environ. Sci. Health A 40, 1457–1466. https://doi.org/10.1081/ESE-200055886.

Aguirre-Sierra, A., Bacchetti-De Gregoris, T., Berná, A., Salas, J.J., Aragón, C., Esteve-Núñez, A., 2016. Microbial electrochemical systems outperform fixed-bed biofilters in cleaning up urban wastewater. Environ Sci (Camb) 2, 984–993. https://doi.org/10.1039/c6ew00172f.

Baek, G., Kim, K.-Y., Logan, B.E., 2021. Impact of surface area and current generation of microbial electrolysis cell electrodes inserted into anaerobic digesters. Chem. Eng. J. 426, 131281. https://doi.org/10.1016/j.cej.2021.131281.

Barnett, D., Arts, I., Penders, J., 2021. microViz: an R package for microbiome data visualization and statistics. J. Open Source Softw. 6, 3201. https://doi.org/10.21105/joss.03201.

Bhat, S.A., Kumar, V., Li, F., Verma, P., 2024. Detection and Treatment of Emerging Contaminants in Wastewater. IWA Publishing. https://doi.org/10.2166/9781789063752.

Bokulich, N.A., Kaehler, B.D., Rideout, J.R., Dillon, M., Bolyen, E., Knight, R., Huttley, G. A., Gregory Caporaso, J., 2018. Optimizing taxonomic classification of marker-gene amplicon sequences with QIIME 2’s q2-feature-classifier plugin. Microbiome 6, 90. https://doi.org/10.1186/s40168-018-0470-z.

Bolyen, E., Rideout, J.R., Dillon, M.R., Bokulich, N.A., Abnet, C.C., Al-Ghalith, G.A., Alexander, H., Alm, E.J., Arumugam, M., Asnicar, F., Bai, Y., Bisanz, J.E., Bittinger, K., Brejnrod, A., Brislawn, C.J., Brown, C.T., Callahan, B.J., Caraballo-Rodríguez, A.M., Chase, J., Caporaso, J.G., 2019. Reproducible, interactive, scalable and extensible microbiome data science using QIIME 2. Nat. Biotechnol. 37, 852–857. https://doi.org/10.1038/s41587-019-0209-9.

Cross, K., Tondera, K., Rizzo, A., Andrews, L., Pucher, B., Darja, I., Karres, N., McDonald, R., 2021. Nature-Based Solutions for Wastewater Treatment: A Series of Factsheets and Case Studies. IWA Publishing. https://doi.org/10.2166/9781789062267.

Directive (EU) 2024/3019 of the European Parliament and of the Council of 27 November 2024 concerning urban wastewater treatment (recast), 2024.
Doherty, L., Zhao, Y., Zhao, X., Hu, Y., Hao, X., Xu, L., Liu, R., 2015. A review of a recently emerged technology: Constructed wetland - Microbial fuel cells. Water Res. https://doi.org/10.1016/j.watres.2015.08.016.
Dotro, G., Langergraber, G., Molle, P., Nivala, J., Puigagut, J., Stein, O., von Sperling, M., 2017. Treatment Wetlands. IWA Publishing. https://doi.org/10.2166/9781780408774.
Du, J., Niu, Y., Wu, H., Konnerup, D., Wu, S., Ramírez-Vargas, C.A., Yang, Y., Brix, H., Arias, C.A., 2022. Effects of electroconductive materials on treatment performance and microbial community structure in biofilter systems with silicone tubings. Chemosphere 307. https://doi.org/10.1016/j.chemosphere.2022.135828.
Fiedler, J., Fuß, R., Glatzel, S., Hagemann, U., Huth, V., Jordan, S., Jurasinski, G., Kutzbach, L., Maier, M., Schäfer, K., Weber, T., Weymann, D., 2022. BEST PRACTICE GUIDELINE Measurement of carbon dioxide, methane and nitrous oxide fluxes between soil-vegetation-systems and the atmosphere using non-steady state chambers. https://doi.org/10.23689/fidgeo-5422.
Garbini, G.L., Barra Caracciolo, A., Grenni, P., 2023. Electroactive Bacteria in Natural Ecosystems and Their Applications in Microbial Fuel Cells for Bioremediation: A Review. Microorganisms 11, 1255. https://doi.org/10.3390/microorganisms11051255.
Ge, S., Wang, S., Yang, X., Qiu, S., Li, B., Peng, Y., 2015. Detection of nitrifiers and evaluation of partial nitrification for wastewater treatment: A review. Chemosphere 140, 85–98. https://doi.org/10.1016/j.chemosphere.2015.02.004.
Gu, Z., Eils, R., Schlesner, M., 2016. Complex heatmaps reveal patterns and correlations in multidimensional genomic data. Bioinformatics 32, 2847–2849. https://doi.org/10.1093/bioinformatics/btw313.
Kadlec, R.H., Wallace, S., 2008. Treatment Wetlands, 2nd edition. CRC Press. https://doi.org/10.1201/9781420012514.
Khramenkov, S.v., Kozlov, M.N., Kevbrina, M.v., Dorofeev, A.G., Kazakova, E.A., Grachev, V.A., Kuznetsov, B.B., Polyakov, D.Yu., Nikolaev, Yu.A., 2013. A novel bacterium carrying out anaerobic ammonium oxidation in a reactor for biological treatment of the filtrate of wastewater fermented sludge. Microbiology (N Y) 82, 628–636. https://doi.org/10.1134/S002626171305007X.
Koukoura, A., Seintos, T., Statiris, E., Barka, E., Gatidou, G., Noutsopoulos, C., Malamis, S., Mamais, D., Masi, F., Rizzo, A., Fountoulakis, M.S., Stasinakis, A.S., 2024. Comparing the performance of microbial electrochemical assisted and aerated treatment wetlands in pilot-scale: Removal of major pollutants and organic micropollutants. Sci. Total Environ. 951, 175550. https://doi.org/10.1016/j.scitotenv.2024.175550.
Lim, N.Y.N., Roco, C.A., Frostegård, Å., 2016. Transparent DNA/RNA Co-extraction Workflow Protocol Suitable for Inhibitor-Rich Environmental Samples That Focuses on Complete DNA Removal for Transcriptomic Analyses. Front. Microbiol. 7. https://doi.org/10.3389/fmicb.2016.01588.
Logan, B.E., Regan, J.M., 2006. Microbial Fuel Cells—Challenges and Applications. Environ. Sci. Technol. 40, 5172–5180. https://doi.org/10.1021/es0627592.
Martin, M., 2011. Cutadapt removes adapter sequences from high-throughput sequencing reads. EMBnet J 17, 10. https://doi.org/10.14806/ej.17.1.200.
Okopi, S., Li, Y., Xu, F., 2024. Biomass Digestion. In: Encyclopedia of Sustainable Technologies. Elsevier, pp. 236–251. https://doi.org/10.1016/B978-0-323-90386-8.00051-6.
Oliva, A., Nguyen, B.L., Mascellino, M.T., D'Abramo, A., Iannetta, M., Ciccaglioni, A., Vullo, V., Mastroianni, C.M., 2013. Sonication of Explanted Cardiac Implants Improves Microbial Detection in Cardiac Device Infections. J. Clin. Microbiol. 51, 496–502. https://doi.org/10.1128/JCM.02230-12.
Panghal, V., Singh, A., Hooda, V., Arora, D., Bhateria, R., Kumar, S., 2025. Recent progress, challenges, and future prospects in constructed wetlands employing biochar as a substrate: a comprehensive review. Environ. Sci. Pollut. Res. https://doi.org/10.1007/s11356-024-35846-7.
Peñacoba-Antona, L., Ramirez-Vargas, C.A., Wardman, C., Carmona-Martinez, A.A., Esteve-Núñez, A., Paredes, D., Brix, H., Arias, C.A., 2022. Microbial Electrochemically Assisted Treatment Wetlands: Current Flow Density as a Performance Indicator in Real-Scale Systems in Mediterranean and Northern European Locations. Front. Microbiol. 13. https://doi.org/10.3389/fmicb.2022.843135.
Peñacoba-Antona, L., Senán-Salinas, J., Aguirre-Sierra, A., Letón, P., Salas, J.J., García-Calvo, E., Esteve-Núñez, A., 2021. Assessing METland® Design and Performance Through LCA: Techno-Environmental Study With Multifunctional Unit Perspective. Front. Microbiol. 12. https://doi.org/10.3389/fmicb.2021.652173.
Prado, A., Berenguer, R., Esteve-Núñez, A., 2019. Electroactive biochar outperforms highly conductive carbon materials for biodegrading pollutants by enhancing microbial extracellular electron transfer. Carbon N Y 146, 597–609. https://doi.org/10.1016/j.carbon.2019.02.038.
Prado, A., Ramírez-Vargas, C.A., Arias, C.A., Esteve-Núñez, A., 2020. Novel bioelectrochemical strategies for domesticating the electron flow in constructed wetlands. Sci. Total Environ. 735. https://doi.org/10.1016/j.scitotenv.2020.139522.
Prado de Nicolás, A., Berenguer, R., Esteve-Núñez, A., 2022. Evaluating bioelectrochemically-assisted constructed wetland (METland®) for treating wastewater: Analysis of materials, performance and electroactive communities. Chem. Eng. J. 440. https://doi.org/10.1016/j.cej.2022.135748.
Pun, Á., Boltes, K., Letón, P., Esteve-Nuñez, A., 2019. Detoxification of wastewater containing pharmaceuticals using horizontal flow bioelectrochemical filter. Bioresour. Technol. Rep. 7, 100296. https://doi.org/10.1016/j.biteb.2019.100296.
R Core Team, 2022. R: A language and environment for statistical computing.
Ramírez-Vargas, C.A., Prado, A., Arias, C.A., Carvalho, P.N., Esteve-Núñez, A., Brix, H., 2018. Microbial electrochemical technologies for wastewater treatment: principles and evolution from microbial fuel cells to bioelectrochemical-based constructed wetlands. Water (Switzerland) 10. https://doi.org/10.3390/w10091128.
Robeson, M.S., O'Rourke, D.R., Kaehler, B.D., Ziemski, M., Dillon, M.R., Foster, J.T., Bokulich, N.A., 2021. RESCRIPt: Reproducible sequence taxonomy reference database management. PLoS Comput. Biol. 17, e1009581. https://doi.org/10.1371/journal.pcbi.1009581.
Rognes, T., Flouri, T., Nichols, B., Quince, C., Mahé, F., 2016. VSEARCH: a versatile open source tool for metagenomics. PeerJ 4, e2584. https://doi.org/10.7717/peerj.2584.
Roy, H., Rahman, T.U., Tasnim, N., Arju, J., Rafid, Md.M., Islam, Md.R., Pervez, Md.N., Cai, Y., Naddeo, V., Islam, Md.S., 2023. Microbial Fuel Cell Construction Features and Application for Sustainable Wastewater Treatment. Membranes (Basel) 13, 490. https://doi.org/10.3390/membranes13050490.
Russel, J., 2024. MicEco: Various functions for microbial community data.
Saeed, T., Miah, M.J., Khan, T., Ove, A., 2020. Pollutant removal employing tidal flow constructed wetlands: Media and feeding strategies. Chem. Eng. J. 382, 122874. https://doi.org/10.1016/j.cej.2019.122874.
Sherertz, R.J., Raad, I.I., Belani, A., Koo, L.C., Rand, K.H., Pickett, D.L., Straub, S.A., Fauerbach, L.L., 1990. Three-year experience with sonicated vascular catheter cultures in a clinical microbiology laboratory. J. Clin. Microbiol. 28, 76–82. https://doi.org/10.1128/jcm.28.1.76-82.1990.
Vymazal, J., 2023. Thirty years of constructed wetlands for municipal wastewater treatment in the Czech Republic. Ecol. Eng. 194, 107054. https://doi.org/10.1016/j.ecoleng.2023.107054.
Vymazal, J., Zhao, Y., Mander, Ü., 2021. Recent research challenges in constructed wetlands for wastewater treatment: A review. Ecol. Eng. 169, 106318. https://doi.org/10.1016/j.ecoleng.2021.106318.
Wang, Q., Liang, Y., Tang, J., Pu, Z., Chen, Y., Huang, L., 2024. Biological mechanisms affecting the release of greenhouse gases from microbial fuel cell-constructed wetland by simultaneously altering structure and electron shuttles. J. Clean. Prod. 466, 142919. https://doi.org/10.1016/j.jclepro.2024.142919.
Wang, X., Tian, Y., Liu, H., Zhao, X., Peng, S., 2019. The influence of incorporating microbial fuel cells on greenhouse gas emissions from constructed wetlands. Sci. Total Environ. 656, 270–279. https://doi.org/10.1016/j.scitotenv.2018.11.328.
Wei, T., López Sepúlveda, M.E., Hernández, S.B., Peñacoba-Antoná, L., Zhao, Y., Núñez, A.E., 2025. Modular bioelectrochemical wetland: A demonstration study for treating urban wastewater. J. Water Process Eng. 70, 106997. https://doi.org/10.1016/j.jwpe.2025.106997.
Weisburg, W.G., Barns, S.M., Pelletier, D.A., Lane, D.J., 1991. 16S ribosomal DNA amplification for phylogenetic study. J. Bacteriol. 173, 697–703. https://doi.org/10.1128/jb.173.2.697-703.1991.
Xia, Z., Wang, Q., She, Z., Gao, M., Zhao, Y., Guo, L., Jin, C., 2019. Nitrogen removal pathway and dynamics of microbial community with the increase of salinity in simultaneous nitrification and denitrification process. Sci. Total Environ. 697, 134047. https://doi.org/10.1016/j.scitotenv.2019.134047.
Xu, H., Song, H.-L., Singh, R.P., Yang, Y.-L., Xu, J.-Y., Yang, X.-L., 2021. Simultaneous reduction of antibiotics leakage and methane emission from constructed wetland by integrating microbial fuel cell. Bioresour. Technol. 320, 124285. https://doi.org/10.1016/j.biortech.2020.124285.
Xu, Z., Hattori, S., Masuda, Y., Toyoda, S., Koba, K., Yu, P., Yoshida, N., Du, Z.-J., Senoo, K., 2024. Unprecedented N 2 O production by nitrate-ammonifying *Geobacteraceae* with distinctive N 2 O isotopocule signatures. mBio 15. https://doi.org/10.1128/mbio.02540-24.
Yadav, A.K., Dash, P., Mohanty, A., Abbassi, R., Mishra, B.K., 2012. Performance assessment of innovative constructed wetland-microbial fuel cell for electricity production and dye removal. Ecol. Eng. 47, 126–131. https://doi.org/10.1016/j.ecoleng.2012.06.029.
Yu, R., Kampschreur, M.J., Loosdrecht, M.C.M. van, Chandran, K., 2010. Mechanisms and Specific Directionality of Autotrophic Nitrous Oxide and Nitric Oxide Generation during Transient Anoxia. Environ. Sci. Technol. 44, 1313–1319. https://doi.org/10.1021/es902794a.
Zhang, L., Liu, Yunlong, Lv, S., Wang, R., Wang, Y., Lin, K., Hu, X., Liu, Yuchen, Dong, Z., Liu, L., 2023. An overview on constructed wetland-microbial fuel cell: Greenhouse gases emissions and extracellular electron transfer. J. Environ. Chem. Eng. 11, 109551. https://doi.org/10.1016/j.jece.2023.109551.
Zhang, L., Pan, W., Xu, C., Du, L., Guo, X., 2026. Greenhouse gas emissions and control measures for constructed wetland: A systematic review. J. Environ. Manag. 397, 128222. https://doi.org/10.1016/j.jenvman.2025.128222.
Zhao, H.-Q., Liu, Q., Wang, Y.-X., Han, Z.-Y., Chen, Z.-G., Mu, Y., 2018. Biochar enhanced biological nitrobenzene reduction with a mixed culture in anaerobic systems: Short-term and long-term assessments. Chem. Eng. J. 351, 912–921. https://doi.org/10.1016/j.cej.2018.06.154.